JOC Article

A DFT Study on the Mechanism of the Annulation Reaction of Trichloronitroethylene with Aniline in the Synthesis of Quinoxalinone-*N*-oxides

Gül A. Özpınar,[†] Safiye S. Erdem,*[,†] Christian Meyer,[‡] and Dieter E. Kaufmann[‡]

Department of Chemistry, Faculty of Science & Letters, Marmara University, Goztepe Campus, 34722 Istanbul, Turkey, and Institut für Organische Chemie, Technische Universität Clausthal, Leibnizstr. 6 D-38678 Clausthal-Zellerfeld, Germany

erdem@marmara.edu.tr

Received February 18, 2009

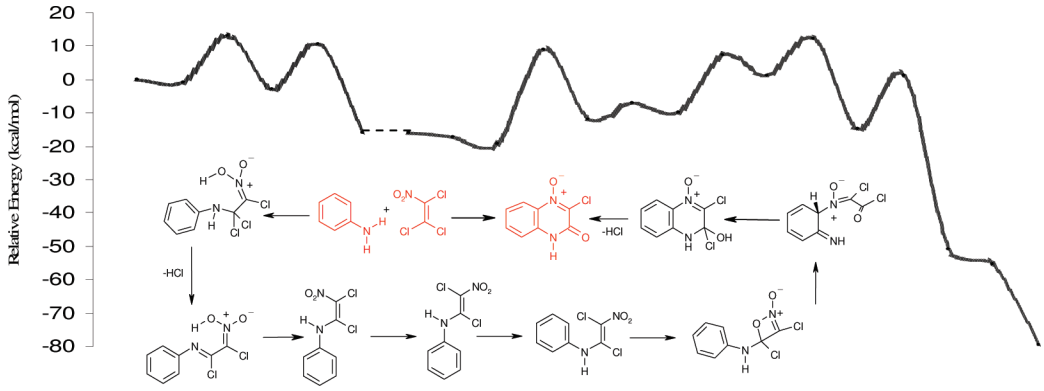

The new annulation reaction of trichloronitroethylene with aniline results in the formation of a quinoxalinone-*N*-oxide derivative. The mechanism of this one-pot annulation reaction between trichloronitroethylene (TCNiE) and anilines has been extensively investigated with B3LYP/6-31+G** methodology. Five different paths (1−5) were proposed and modeled by using this method. These paths were compared in terms of the activation energies of their rate-determining steps and in regard to the experimental findings. Paths 3 and 5, proceeding via four-membered heterocyclic rings, were found to be the most plausible paths with activation energies of 32 and 29 kcal/mol for the rate-determining steps, respectively. The effects of substituent, solvent, temperature, and computational method on these steps were also investigated. The results showed that path 5 is the most plausible mechanism for the annulation reaction of trichloronitroethylene with aniline.

1. Introduction

The chemistry of nitro compounds has been extensively studied over the years. Interest in these compounds arises from their being versatile precursors for the synthesis of diverse functionalized compounds.[1] In particular, nitroalkenes are powerful electrophiles that undergo conjugate addition reactions with nucleophiles and radicals. In addition, they act as dienophiles in cycloaddition reactions. These processes may be used to readily assemble molecules with extended carbon frameworks.[1b] Heteroatom-substituted nitroalkenes are particularly useful compounds for the controlled synthesis of heterocyclic or related molecules.[2−5] Halogenated nitroalkenes as reactive electrophiles undergo Michael addition reactions with nucleophiles. In these reactions, the halogen substituent is usually displaced after the Michael addition. These processes have been used to prepare three-, four-, five-, and six-membered heterocyclic rings.[6] The reactions of polyhalogenated nitrobutadiene systems as members of halonitroalkenes have been

[†] Marmara University.
[‡] Technische Universität Clausthal.

(1) (a) Bauer, H. H.; Urbas, L. In *The Chemistry of the Nitro and Nitroso Group*; Feuer, H. Ed.; Interscience: New York, 1970; Part 2, pp 75−200. (b) Denmark, S. E.; Thorarensen, A. *Chem. Rev.* **1996**, *96*, 137.
(2) Ioffe, S. L.; Leont'eva, L. M.; Tartakovski, V. A. *Russ. Chem. Rev. (Engl. Transl.)* **1977**, *46*, 872.
(3) Seebach, D.; Colvin, E. W.; Lehr, F.; Weller, T. *Chimia* **1979**, *39*, 1.
(4) Perekalin, V. V. *J. Org. Chem. U.S.S.R. (Engl. Transl.)* **1985**, *21*, 1011.
(5) Barrett, A. G. M.; Graboski, G. G. *Chem. Rev.* **1986**, *86*, 751.
(6) Barrett, A. G. M. *Chem. Soc. Rev.* **1991**, *20*, 95.

10.1021/jo9003629 CCC: $40.75
Published on Web 06/04/2009

SCHEME 1. Reactions[a] of Trichloronitroethylene[13−20]

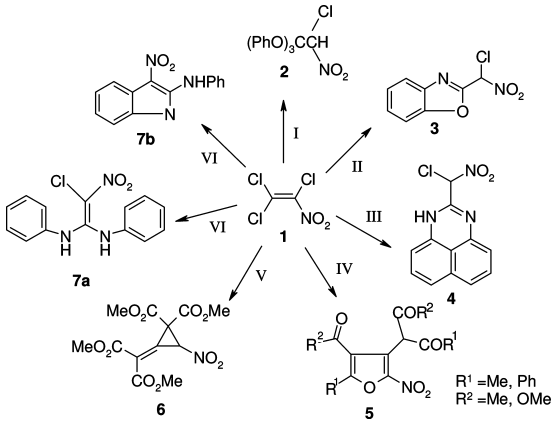

[a] Reagents: (I) NaOMe, 3 equiv of PhOH, MeOH, 0−5°C; (II) 2-$H_2NC_6H_4$−OH, NaOMe, MeOH; (III) 1,8-diaminonaphthalene, Et_2O, 10 °C; (IV) $R_1COCH_2COR_2$, NaOMe; (V) $(MeO_2C)_2CH_2$, NaOMe, MeOH; (VI) 2 equiv of $PhNH_2$, Et_2O, −20 °C; (VII) 1. 2 equiv of $PhNH_2$, Et_2O, 5 °C; 2. EtOH, 78 °C.

extensively studied.[7−12] However, the synthetic applications of halonitroethylenes,[6] especially trichloronitroethylene (TCNiE) (**1**), are rare in the literature relative to those of halonitrobutadiene. Trichloronitroethylene (**1**) is a very useful reagent for preparing orthoesters through its reactions with phenols and alcohols under basic conditions.[13] The preparation of the orthoacetate (**2**) proceeds via a triple Michael addition to **1** and double loss of chloride (Scheme 1). TCNiE (**1**) is also used to prepare heterocyclic rings such as benzoxazole,[14] 1*H*-perimidine,[15] furan derivatives,[16,17] methylene cyclopropane,[18] bis(phenylamino)chloronitroethylene,[19] and indole[20] derivatives (Scheme 1). It is known that these reactions occur via a double addition−elimination mechanism (**3** and **4**) and further displacement of the α-chloride (**5**, **6**, and **7**).

It is interesting that TCNiE gives two different types of product (**7a** or **7b**) in its reactions with aniline at different temperatures (−20 and 5 °C), although they have the same addition ratio (1:2). Recently, a new annulation reaction of trichloronitroethylene (**1**) with aniline (**8**) (Scheme 2) was

SCHEME 2. Annulation Reaction of Trichloronitroethylene with Aniline at 40 °C

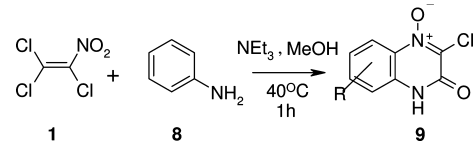

SCHEME 3. Quinoxalinone-*N*-oxide Derivatives Synthesized[23−33]

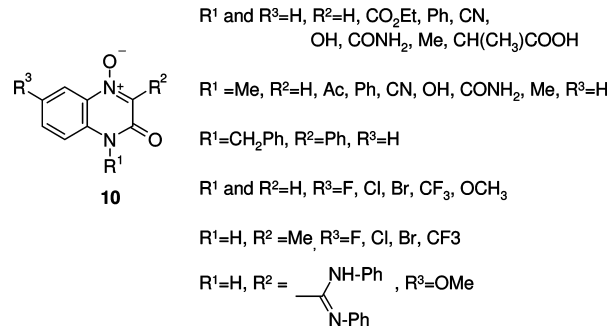

reported by Kaufmann et al.[21,22] With a 1:1 ratio of **1/8** and in the presence of triethylamine, they observed the formation of a new quinoxalinone-*N*-oxide derivative (**9**) at 40 °C and stated that product **9** precipitated completely at the end of the reaction and that single crystals could not be obtained by recrystallization. In order to verify the formation of the quinoxalinone-*N*-oxide structure, they used the X-ray structure of its derivative obtained by the substitution of the Cl atom at the 3-position in **9** with a long chain thiol group. It was also reported that the yield of the annulation reaction depended on several parameters such as the temperature, the solvent, and the substitution pattern of the aniline (for instance, N-substituted anilines do not give the annulation reaction) and that the reaction is exothermic.

One important feature of this annulation reaction is the synthesis of a new quinoxalinone-*N*-oxide derivative (**9**). Quinoxalinone-*N*-oxide derivatives reported in the literature[23−33] so far are given in Scheme 3. Additionally, the ability of substitution of the Cl atom at the 3-position allows one to derive new quinoxalinone-*N*-oxides easily. Since it is well-known that the quinoxalinone derivatives exhibit biological activity such as antimicrobial (against several bacteria, viruses, fungi, etc.), anxiolytic, deconditioning, analgesic, antispastic, antiallergic, antithrombotic, anticancer activity and act as growth promoters, potential carcinogenic and antitumor agents,[34−50] this new quinoxalinone derivative (**9**) is also expected to show biological activity.

(7) Kaberdin, R. V.; Potkin, V. I.; Zapol'skii, V. A. *Russ. Chem. Rev.* **1997**, *66*, 827.
(8) Zapol'skii, V. A.; Namyslo, J. C.; Adam, A. E. W.; Kaufmann, D. E. *Heterocycles* **2004**, *63*, 1281.
(9) Zapol'skii, V. A.; Namyslo, J. C.; Blaschkowski, B.; Kaufmann, D. E. *Synlett* **2006**, *20*, 3464.
(10) Zapol'skii, V. A.; Namyslo, J. C.; Gjikaj, M.; Kaufmann, D. E. *ARKIVOC* **2007**, 76.
(11) Zapol'skii, V. A.; Namyslo, J. C.; Gjikaj, M.; Kaufmann, D. E. *Synlett* **2007**, *10*, 1507.
(12) Zapol'skii, V. A.; Namyslo, J. C.; Altug, G.; Gjikaj, M.; Kaufmann, D. E. *Synthesis* **2008**, *2*, 304.
(13) Buevich, V. A.; Nakova, N. *J. Org. Chem. U.S.S.R. (Engl. Transl.)* **1977**, *13*, 2431.
(14) Buevich, V. A.; Rudchenko, V. V.; Grineva, V. S.; Perekalin, V. V. *J. Org. Chem. U.S.S.R. (Engl. Transl.)* **1979**, *15*, 2031.
(15) Buevich, V. A.; Nakova, N. Zh.; Kempter, G.; Perekalin, V. V. *J. Org. Chem. U.S.S.R. (Engl. Transl.)* **1977**, *13*, 2430; *Zh. Org. Khim* **1977**, *13*, 2618−2619.
(16) Buevich, V. A.; Grineva, V. S.; Deiko, L. I.; Perekalin, V. V. *J. Org. Chem. U.S.S.R. (Engl. Transl.)* **1978**, *14*, 2031.
(17) Buevich, V. A.; Deiko, L. I.; Perekalin, V. V. *J. Org. Chem. U.S.S.R. (Engl. Transl.)* **1981**, *17*, 1175.
(18) Buevich, V. A.; Deiko, L. I.; Volynskii, V. E. *J. Org. Chem. U.S.S.R. (Engl. Transl.)* **1980**, *16*, 2055.
(19) Francotte, E.; Verburggen, R.; Viehe, H. G.; Meerssche, M. V.; Germain, G.; Declercq, J. P. *Bull. Soc. Chim. Belg.* **1978**, *87*, 693.
(20) Buevich, V. A.; Rudchenko, V. V.; Perekalin, V. V. *Khim. Geterotsikl. Soedin.* **1976**, 1429.
(21) Meyer, C. *Anellierte Heterocyclen durch die Reaktion von Trichloronitroethylene mit (hetero)aromatischen Aminen*; Diplomarbeit, TU Clausthal: Germany, 2004.
(22) Meyer, C.; Zapol'skii, V. A.; Adam, A. E. W.; Kaufmann, D. E. *Synthesis* **2008**, 2575.
(23) Cazaux, L.; Faher, M.; Picard, C.; Tisnés, P. *Can. J. Chem.* **1993**, *71*, 2007.
(24) Toman, J.; Klicnar, J. *Collect. Czech. Chem. Commun.* **1986**, *51*, 419.
(25) Toman, J.; Klicnar, J. *Collect. Czech. Chem. Commun.* **1984**, *49*, 976.
(26) Toman, J.; Klicnar, J.; Macháček, V. *Collect. Czech. Chem. Commun.* **1978**, *43*, 2179.
(27) Tennant, G. *J. Chem. Soc.* **1963**, 2428.
(28) Tennant, G. *J. Chem. Soc.* **1964**, 1986.
(29) Tennant, G. *J. Chem. Soc.* **1964**, 2666.
(30) Sakata, G.; Makino, K.; Moritomo, K. *Heterocycles* **1985**, *23*, 143.
(31) Makino, K.; Sakata, G.; Moritomo, K. *Heterocycles* **1985**, *23*, 2069.
(32) Argilagos, D. M.; Linden, A.; Heimgartner, H. *Helv. Chim. Acta* **1999**, *82*, 238.
(33) Brown, D. J. In *Chemistry of Heterocyclic Compounds: Quinoxalines: Suppl. II*; Taylor, E. C., Wipf, P. Eds.; Wiley: New York, 2004; Vol. 61.

SCHEME 4. Path 1 and Path 2

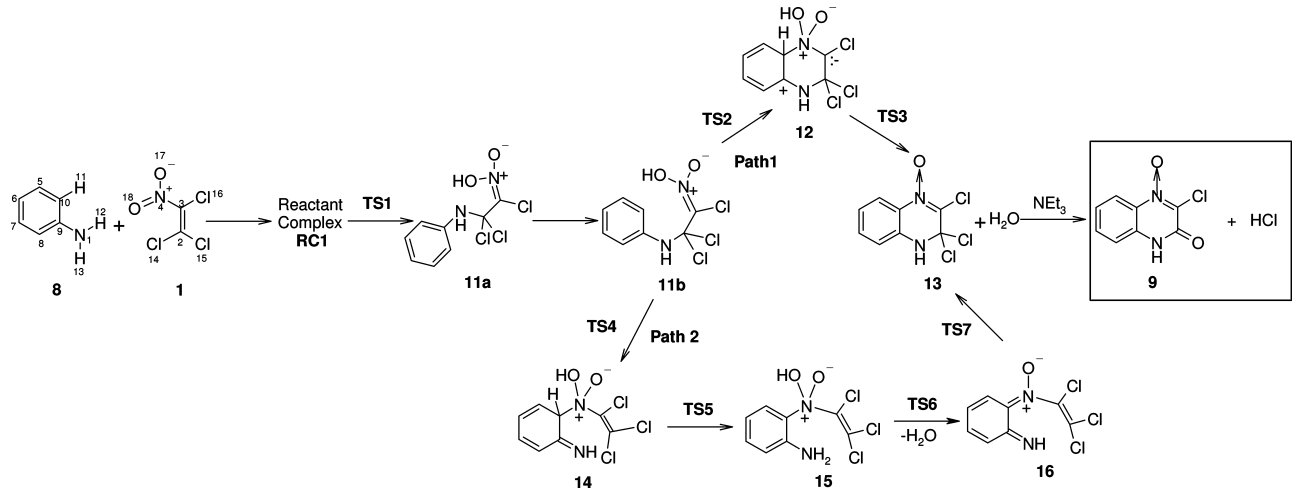

The most important question in the annulation reaction (Scheme 2) regards the mechanism. Kaufmann et al.[21,22] stated that the reaction starts with a Michael addition of the aromatic amine at the C2 position of **1** to form an intermediate such as **11a** (Scheme 4), whereas the detailed mechanism of the formation of product **9** remains unclear. Hence, in the present work, we aimed to enlighten the mechanism of this annulation reaction theoretically. A detailed understanding of the mechanism of this reaction is expected to guide in the design of reactions related to the chemistry of halonitroethylene systems.

Kaufmann et al.[21] proposed two different mechanisms proceeding through electrophilic aromatic substitution (path 1) and aza-Cope rearrangement (path 2), both shown in Scheme 4. In addition to these mechanisms, three different paths depicted in Scheme 5 were also considered in this study and modeled by using density functional theory.[51] In this paper, these five paths are compared with regard to the activation energies of their rate-determining steps and in relation to experimental findings, and the plausibility of the paths is discussed.

2. Computational Methodology

2.1. Choice of Computational Method and Basis Set. In order to choose an appropriate computational level, we calculated the conformational energy change of *N*-hydroxymethylene nitrone (Scheme 6), which mimics intermediates **11a**−**c**, **21**, and **22** by using different computational methods B3LYP[52,53] and MP2[54] involving various basis sets and by a complete basis set model (CBS-QB3).[55]

The conformational energy changes of the model reaction in Scheme 6 at different computational levels are listed in Table 1. We used the energy obtained from the CBS-QB3 method as a reference since this method yields very accurate energies. We observed that MP2/6-311+G** gave the closest result to CBS-QB3. Additional splitting of valence orbitals or inclusion of a second set of diffusion functions to basis set (6-31+G**) decreases the energy difference by only 10 and 5% for MP2/6-311+G** and B3LYP/6-311+G**, respectively. Since MP2 and B3LYP computations predicted very similar energies, we decided to use B3LYP as a compromise between accuracy and computational cost.

In theoretical studies[56,57] on the reactions of structures similar to the reactant (**1**) and the intermediates (**11**, **21**, and **22**) such as nitroethylene and methylene nitrone, it was reported that hybrid density functional methods (especially B3LYP) with a moderate basis set produced good geometries and showed the best performance for reaction enthalpies. It was also stated that single point calculations with larger basis sets did not significantly improve the energy values obtained with a moderate basis set, and hybrid DFT methods were quite reliable in predicting the activation barriers for cycloadditions and for rearrangement and hydrogen abstraction reactions.[58] The proposed mechanisms in the present study include these reaction types. The basis set used should include the polarization function for the hydrogen atom and the diffuse function for charged structures in Schemes 4 and 5. Therefore, 6-31+G** was chosen as an appropriate basis set. This basis set was also recommended for calculating transition state geometries and barrier heights.[59]

(34) Carta, A.; Piras, S.; Loriga, G.; Paglietti, G. *Mini-Rev. Med. Chem* **2006**, *6*, 1.
(35) Ries, U. J.; Priepke, H. W. M.; Hauel, N. H.; Handschuh, S.; Mihm, G.; Stassen, J. M.; Wienen, W.; Nar, H. *Bioorg. Med. Chem. Lett.* **2003**, *13*, 2297.
(36) Carta, A.; Sanna, P.; Gherardini, L.; Usai, D.; Zanetti, S. *Il Farmaco* **2001**, *56*, 933.
(37) Dudash, J., Jr.; Zhang, Y.; Moore, J. B.; Look, R.; Liang, Y.; Beavers, M. P.; Conway, B. R.; Rybczynski, P. J.; Demarest, K. T. *Bioorg. Med. Chem. Lett.* **2005**, *15*, 4790.
(38) Willardsen, J. A.; Dudley, D. A.; Cody, W. L.; Chi, L.; McClanahan, T. B.; Mertz, T. E.; Potoczak, R. E.; Narasimhan, L. S.; Holland, D. R.; Rapundalo, S. T.; Edmunds, J. J. *J. Med. Chem.* **2004**, *47*, 4089.
(39) Carta, A.; Sanna, P.; Loriga, M.; Setzu, M. G.; La Colla, P.; Loddo, R. *Il Farmaco* **2002**, *57*, 19.
(40) Carta, A.; Loriga, M.; Zanetti, S.; Sechi, L. A. *Il Farmaco* **2003**, *58*, 1251.
(41) Sana, P.; Carta, A.; Loriga, M.; Zanetti, S.; Sechi, L. *Il Farmaco* **1999**, *54*, 161.
(42) Sana, P.; Carta, A.; Loriga, M.; Zanetti, S.; Sechi, L. *Il Farmaco* **1999**, *54*, 169.
(43) Obafemi, C. A.; Akinpelu, D. A. *Phosphorus, Sulfur Silicon* **2005**, *180*, 1795.
(44) Katrizky, A. R. Ed. *Comprehensive Heterocyclic Chemistry*; Pergamon: Oxford, 1984; Vol. 1, p 220.
(45) Figdor, G. K.; Hobbs, D. C. *Can. J. Chem.* **1980**, *58*, 1957.
(46) Suter, W.; Rosselet, A.; Knüsel, F. *Antimicrob. Agents Chemother.* **1978**, *13*, 770.
(47) Nakahara, W.; Fukuoka, F.; Sugimura, T. *Gann.* **1957**, *48*, 129.
(48) Shirasu, Y. *Proc. Soc. Exp. Biol. Med.* **1965**, *118*, 812.
(49) Kawazoe, Y.; Tachibana, M.; Aoki, K.; Nakahara, W. *Biochem. Pharmacol.* **1967**, *16*, 631.
(50) Ganley, B.; Chowdhury, G.; Bhansali, J.; Daniels, J. S.; Gates, K. S. *Bioorg. Med. Chem.* **2001**, *9*, 2395.
(51) Parr, R. G.; Yang, W. *Density-Functional Theory of Atoms and Molecules*; Oxford University Press: New York, 1989.
(52) Becke, A. D. *J. Chem. Phys.* **1993**, *98*, 5648.
(53) Lee, C.; Yang, W.; Parr, R. G. *Phys. Rev. B* **1988**, *37*, 785.
(54) Mø´ller, C.; Plesset, M. S. *Phys. Rev.* **1934**, *46*, 618.
(55) Montgomery, J. A.; Frisch, M. J.; Ochterski, J. W.; Petersson, G. A. *J. Chem. Phys.* **1999**, *110*, 2822.
(56) Gindulyté, A.; Massa, L.; Huang, L.; Karle, J. *J. Phys. Chem. A* **2005**, *109*, 11040.
(57) Ess, D. H.; Houk, K. N. *J. Phys. Chem. A* **2005**, *109*, 9542.

SCHEME 5. Paths 3, 4, and 5

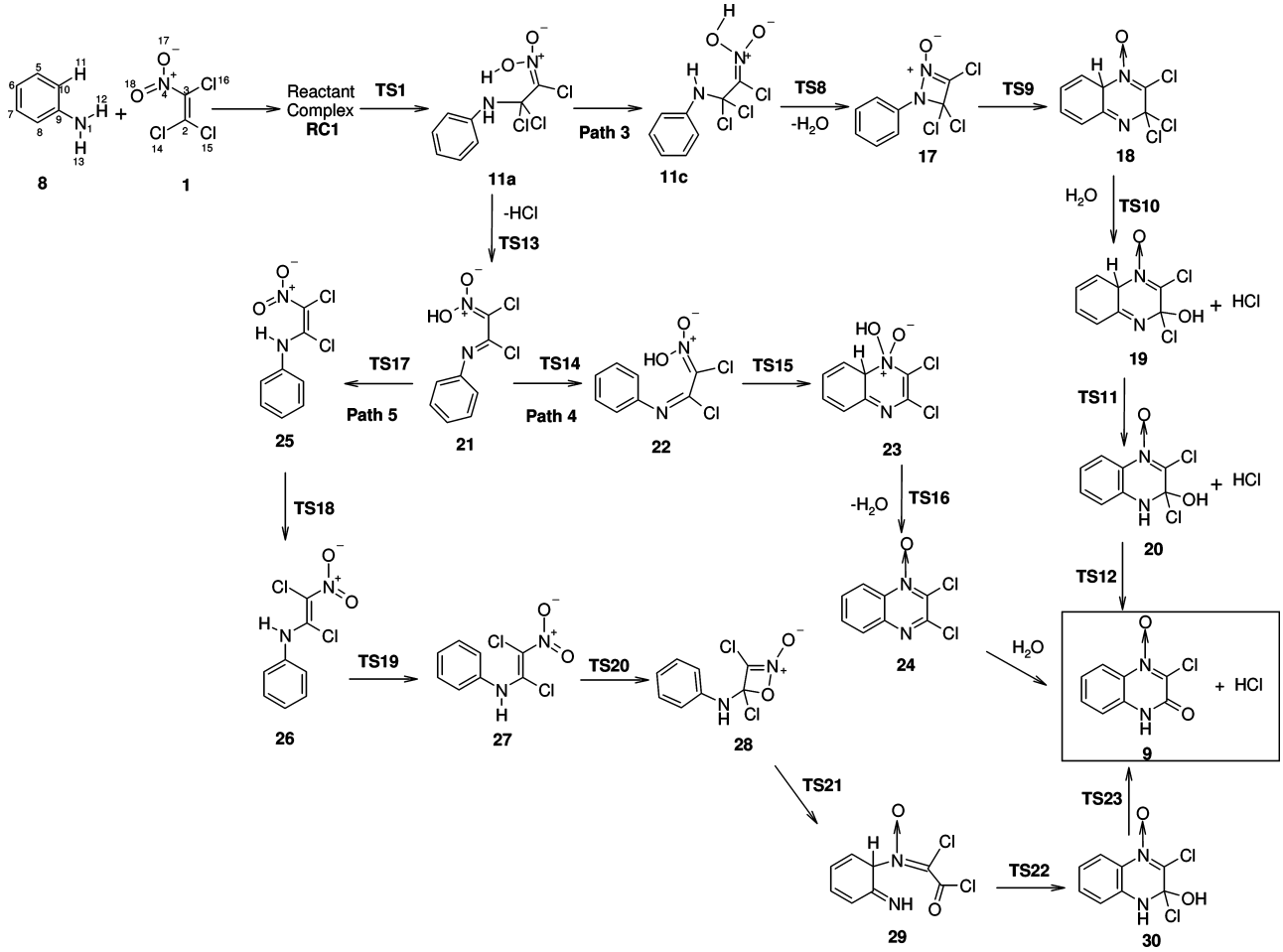

SCHEME 6. Conformational Equilibrium Modeled

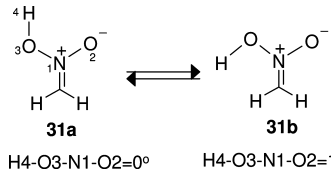

TABLE 1. Total Energy Differences (kcal/mol) between Conformations of *N*-Hydroxymethylene Nitrone

computational levels	ΔE
CBS-QB3	6.51
MP2/6-31G*//HF/6-31G*	7.86
MP2/6-31+G*//HF/6-31+G*	7.77
MP2/6-311+G*//HF/6-311+G*	7.40
MP2/6-311++G*//HF/6-311++G*	7.44
MP2/6-31G**//HF/6-31G**	7.56
MP2/6-31+G**//HF/6-31+G**	7.42
MP2/6-311+G**//HF/6-311+G**	6.58
MP2/6-311++G**//HF/6-311++G**	6.58
B3LYP/6-31G*	7.74
B3LYP/6-31+G*	7.70
B3LYP/6-311+G*	7.64
B3LYP/6-311++G*	7.65
B3LYP/6-31G**	7.60
B3LYP/6-31+G**	7.54
B3LYP/6-311+G**	7.08
B3LYP/6-311++G**	7.11

2.2. Computations. Calculations were performed with the Gaussian 03[60] and Gaussian 98[61] program packages. On the basis of the modeling study given in Scheme 6, the B3LYP/6-31+G** level was chosen and used throughout the present work. The geometries of all stationary points in the proposed reaction paths were optimized at this level. Transition states were located by the traditional transition optimizations with the Berny algorithm[62] or the synchronous transit and quasi-Newton (STQN)[63] method. Forward and backward intrinsic reaction coordinate[64] (IRC) computations were carried out at the same level to connect the transition states to the reactants and the products. Analytic computations of vibrational frequencies in the harmonic approximation were used to characterize the nature of the transition states (one imaginary frequency) and the local minima (no imaginary frequency). Thermal corrections to the zero point energy (ZPE), enthalpy, and Gibbs free energy were calculated at 298.15 K and 1 atm. The activation energies for each step in the pathways were computed, and the rate-determining step of each path was determined. Calculated thermodynamic data were used to examine the effect of temperature (at 40 °C), solvent (methanol), computational

(58) (a) Jursic, B. S. *J. Mol. Struct. (THEOCHEM)* **1998**, *423*, 189. (b) Jursic, B. S. *J. Mol. Struct. (THEOCHEM)* **1995**, *358*, 139. (c) Jursic, B. S. *J. Mol. Struct. (THEOCHEM)* **1995**, *357*, 243. (d) Jursic, B. S. *J. Mol. Struct. (THEOCHEM)* **1996**, *365*, 275.
(59) (a) Lynch, B. J.; Truhlar, D. G. *J. Phys. Chem. A* **2002**, *106*, 842. (b) Lynch, B. J.; Truhlar, D. G. *J. Phys. Chem. A* **2001**, *105*, 2936.
(60) Frisch, M. J.; et al. *Gaussian 03*, revision D.01; Gaussian, Inc.: Wallingford CT, 2004.
(61) Frisch, M. J.; et al. *Gaussian 98*, revision A.8; Gaussian, Inc.: Pittsburgh PA, 1998.
(62) Peng, C.; Ayola, P. Y.; Schlegel, H. B.; Frisch, M. J. *J. Comput. Chem.* **1996**, *17*, 49.
(63) Peng, C.; Schlegel, H. B.; Frisch, M. J. *Isr. J. Chem.* **1994**, *33*, 449.
(64) Gonzalez, C.; Schlegel, H. B. *J. Chem. Phys.* **1989**, *20*, 2514.

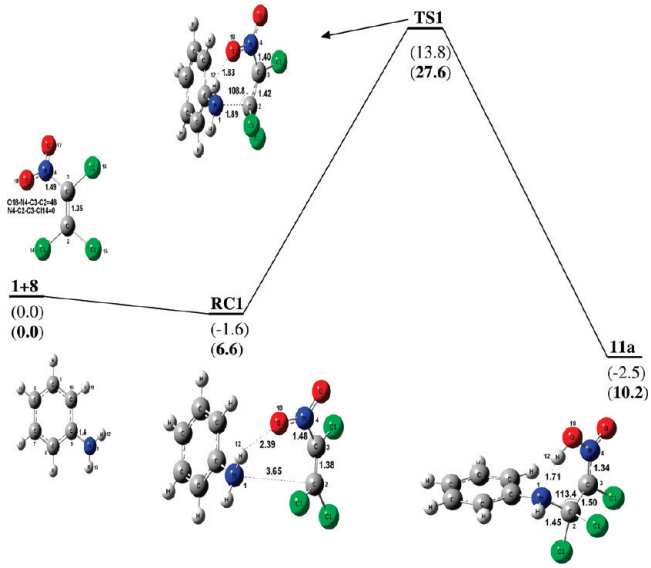

FIGURE 1. Energetics [ZPE corrected energy and Gibbs energy (bold), (kcal/mol)] and optimized structures of reactants, reactant complex, transition state, and intermediate for the Michael addition of TCNiE (**1**) to aniline (**8**).

methods [PBE1PBE,[65] BLYP,[66] B3PW91,[67] MPW1PW91,[68] MPW1K,[59] MP2(SP)], and substituent (at the *para* and *meta* positions of aniline) on the rate-determining steps of the paths chosen as the most plausible. The computations of solvent effect were performed by using the polarizable continuum model[69] (PCM) as single point energies. Thermodynamic corrections obtained from frequency calculations in the gas phase were added to the electronic energy obtained from single point PCM calculations in order to compute ZPE corrected energy, enthalpy, and Gibbs energy values in the solution phase.

3. Results and Discussion

We modeled five distinct paths leading to the synthesis of new quinoxalinone-*N*-oxides, following the nucleophilic addition of aniline (**8**) to TCNiE (**1**), as shown in Schemes 4 and 5.

3.1. Initial Step (Michael Addition). The Michael addition of aniline (**8**) to TCNiE (**1**) takes place through the transition state **TS1**. Normal mode analysis shows that the structure has only one imaginary frequency of 295.9*i* cm^{-1}. IRC calculations were performed to confirm that **TS1** connects the reactant complex (**RC1**) to intermediate **11a**, as shown in Figure 1. The activation energy was calculated as 13.8 kcal/mol, while the Gibbs free energy of activation was found to be 27.6 kcal/mol in the gas phase. This large difference between energies arises from the effect of entropy on the bimolecular addition. When the reaction is treated as unimolecular, Gibbs free energy of activation decreases to 21.0 kcal/mol. The existence of a hydrogen bond (1.8 Å) between H12 and O18 contributes to the stabilization of **TS1** and reduces the activation barrier. IRC calculation toward reactants leads to a prereactive complex **RC1** stabilized by a N1−H12···O18 hydrogen bond with a distance of 2.39 Å. Forward IRC calculation leads to intermediate **11a**, which is also stabilized by the strong N1···H12−O8 hydrogen bond with a distance of 1.71 Å.

(65) Perdew, J. P.; Burke, K.; Ernzerhof, M. *Phys. Rev.* **1996**, *77*, 3865.
(66) (a) Becke, A. D. *J. Chem. Phys.* **1996**, *104*, 1040. (b) Adamo, C.; Barone, V. *Chem. Phys. Lett.* **1997**, *274*, 242.
(67) Perdew, J. P.; Burke, K.; Wang, Y. *Phys. Rev.* **1996**, *B54*, 16533.
(68) Adamo, C.; Barone, V. *J. Chem. Phys.* **1998**, *108*, 664.
(69) Miertus, S.; Scrocco, E.; Tomasi, J. *J. Chem. Phys.* **1981**, *55*, 117.

SCHEME 7

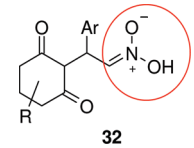

32

The similar formation of the C═NO_2H moiety in **11** was proposed by Ishikawa et al.[70] They performed the reaction of 1-aryl-2-nitroethylene derivatives with cyclohexane-1,3-diones under basic conditions at room temperature, which resulted in benzofuran derivatives. For the addition of 1-aryl-2-nitroethylene to cyclohexane-1,3-dione, structure **32**, shown in Scheme 7, was proposed in the first step of the reaction mechanism.

3.2. Path 1. Path 1 is based on electrophilic aromatic substitution. After the Michael addition discussed above, this path follows four steps: conformational change from **11a** to **11b**, electrophilic aromatic substitution, aromatization through water elimination, and hydrolysis of the *gem*-dichloride moiety (Scheme 4). Unfortunately, the computational level used failed to optimize the transition state **TS2** and intermediate **12**, probably because of the zwitterionic character of these structures in the gas phase. The HF/6-31G* method (available in Supporting Information) was successful in locating these structures but resulted in an extremely high activation barrier (about 94 kcal/mol). Single point energy calculations with B3LYP/6-31+G** on structures optimized with HF decreased the barrier by 20 kcal/mol, which was still very high. Therefore, this mechanism was ruled out, and the remaining steps were not modeled.

3.3. Path 2. After the formation of **11b**, the proposed path 2 (Figure 2) involves the following steps: aza-Cope rearrangement, 1,3-H shift, elimination of water, cyclization, and hydrolysis of geminal dichloride. Transition state **TS4** in the aza-Cope rearrangement step involves simultaneous formation of the C10−N4 bond and cleavage of the N1−C2 bond. These

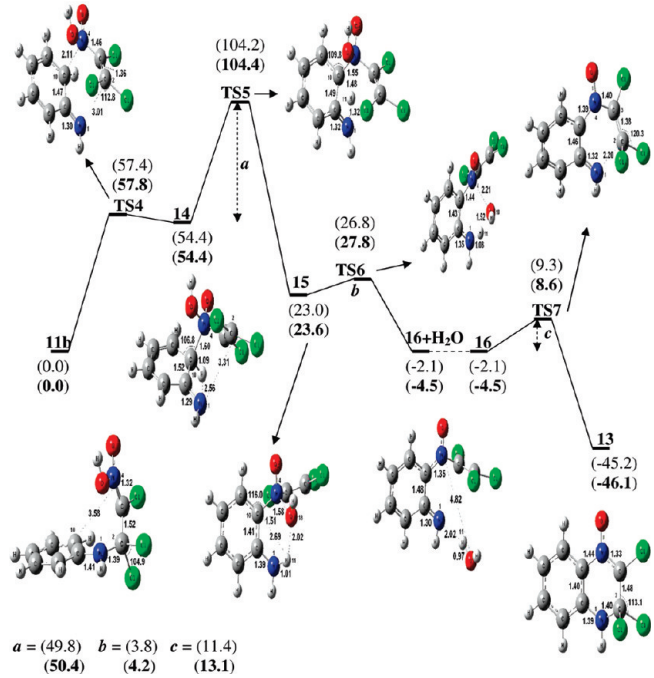

FIGURE 2. Energetics [ZPE corrected energy and Gibbs energy (bold), (kcal/mol)] and optimized structures in path 2.

SCHEME 8

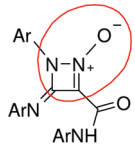

33

bond distances for **11b**, **TS4**, and **14** are shown in Figure 2. The C10−N4 bonds are 3.58, 2.11, and 1.60 Å, while the N1−C2 bonds are 1.39, 3.01, and 3.31 Å for **11b**, **TS4**, and **14**, respectively. For the C10 atom, conversion of hybridization from sp^2 to sp^3, which exhibits a high activation barrier of 57.8 kcal/mol and is very endothermic by 54.4 kcal/mol, is clearly observed. In transition state **TS5** of the second step, H11 migrates from the C10 to the N1 atom, thus, the benzene ring gains its aromaticity back. This step also has a very high barrier of 50.4 kcal/mol, whereas it is quite exothermic with −30.8 kcal/mol since product **15** is stabilized by aromatization. The C10−H11 bond is 1.09 Å for intermediate **14** and is elongated in **TS5** (1.48 Å). The third step of this path is water elimination from **15**, which takes place through transition state **TS6** and has an extremely low free energy of activation of 4.2 kcal/mol. It is also exothermic by −28.1 kcal/mol. The N4−OH bond becomes longer (2.21 Å for **TS6**), and the hydroxy group picks up the H12 atom from the N1 atom, resulting in the elimination of a water molecule. Forward IRC calculation from **TS6** shows the existence of an intermediate complex (**16**+$\mathbf{H_2O}$) involving an intermolecular hydrogen bond (N1···H11−O18) with a distance of 2.02 Å. The next step is the cyclization of intermediate **16**, which is exothermic (−43.7 kcal/mol) and requires an energy barrier of only 11 kcal/mol. The N1−C2 bond re-forms with a length of 2.20 Å in **TS7** and 1.40 Å in **13**. The last step of this path, which is the hydrolysis of the *gem*-dichloride moiety in **13**, was not modeled since it is very well-known that this type of hydrolysis occurs easily under basic conditions.[71]

As a result, the overall reaction enthalpy up to intermediate **13** is predicted to be −46.1 kcal/mol, which indicates a highly exothermic reaction. This result supports the experimental finding that the reaction is exothermic. However, path 2 cannot explain why N-substituted anilines do not give the reaction since one of the hydrogen atoms at N1 of aniline stays bonded to N1 in all steps of this path. In addition, the aza-Cope rearrangement step with an activation barrier of 57.8 kcal/mol is quite high, and it is considered to be the rate-determining step. Nevertheless, the barrier of the hydrogen migration step (relative to **11b**) involving **TS5** is extremely larger (104.4 kcal/mol). Therefore, such a mechanism is not likely to occur.

3.4. Path 3. Path 3 starts with the elimination of water from **11c** involving a hydrogen bond between H13 and O18 (Scheme 5). Relative energy values for this path are presented in Figure 3, and the geometrical parameters of the optimized structures are given in Figure 4. **TS8** is the transition state for water elimination, in which the σ bonds N1−H13 and N4−O18 break while the N1−N4 and H13−O18 bonds form to give a four-membered cyclic intermediate **17**, namely, 1,4-dihydro-1,2-diazete or a diazacyclobutene derivative. A similar type of intermediate, **17**, was also proposed as the intermediate in the formation mechanism of 1,2,5-oxadiazole derivatives by desulfurization of substituted 2-aryl-3-phenylamino-4-nitro-5-aryliminoisothiaozole derivatives.[32] (Scheme 8).

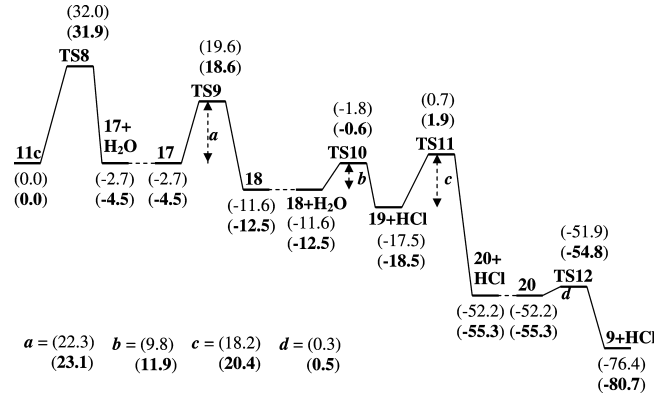

FIGURE 3. Energetics [ZPE corrected energy and Gibbs energy (bold), (kcal/mol)] and optimized structures in path 3.

Forward IRC computation of **TS8** produces an intermediate complex, **17**+$\mathbf{H_2O}$, in which the water molecule participates in hydrogen bonding with the N1 atom. The N1−H13, N4−O18, and N1−C2 bonds elongate from 1.01, 1.42, and 1.39 Å in **11c** to 2.2, 4.05, and 1.50 Å in **17**, respectively, while the O18−H13 and N1−N4 bonds become shorter from 2.0 and 2.97 Å in **11c** to 0.97 and 1.50 Å in **17**, respectively, as shown in Figure 4. The water elimination (WE) step is slightly exothermic, about −4.5 kcal/mol, and has an activation barrier of 31.9 kcal/mol. The next step is electrophilic aromatic substitution of **17** through **TS9**, in which the N4 atom is bonded to C10 while the N1−N4 bond breaks in order to produce bicyclic intermediate **18**. The length of the C10−N4 bond in structures **17**, **TS9**, and **18** is 2.92, 2.8, and 1.51 Å, respectively. The Gibbs free energy of activation for this step is 23.1 kcal/mol, and the Gibbs free energy of reaction is about −8.0 kcal/mol. After the electrophilic aromatic substitution step, hydrolysis of the geminal dichloride moiety in **18** takes place. **TS10** is the transition state of the hydrolysis in which the O18 atom of the water molecule attacks the carbon atom (C2) bonded to two chloro substituents, and HCl is eliminated from the structure. Reverse and forward IRC calculations for **TS10** produce intermediate complexes of **18**+$\mathbf{H_2O}$ and **19**+**HCl**. The C2−O18 bond distance is 3.98, 1.73, and 1.40 Å, while the Cl14−H13 bond length is 2.55, 1.76, and 1.30 Å in **18**+$\mathbf{H_2O}$, **TS10**, and **19**+**HCl**, respectively. This step requires a Gibbs free activation energy of about 11.9 kcal/mol and is exothermic by −6.0 kcal/mol. The separated HCl behaves as a bridge and assists the hydrogen transfer from C10 to N1 in **TS11**, in which the H11 atom bonded to C10 migrates to the Cl14 (2.35 Å) atom while H13 gets closer to the N1 atom (1.15 Å). Another intermediate complex, **20**+**HCl**, is produced at the end of this step. The Gibbs activation energy of this step is predicted to be 20.4 kcal/mol. The calculated reaction energy is highly exothermic by −36.8 kcal/mol since the benzene ring gains its aromaticity back in bicyclic intermediate **20**. The hydrolysis of the geminal dichloride moiety is completed in the last step, in which the second HCl elimination from **20** takes place through **TS12** to form the ketone moiety of target product **9**. This step is also exothermic by −25.4 kcal/mol since product **9** is stabilized by π-electron delocalization in the heterocyclic ring. The C2−O18 bond distance is 1.36,

(70) Ishikawa, T.; Miyahara, T.; Asakura, M.; Higuchi, S.; Miyauchi, Y.; Saito, S. *Org. Lett.* **2005**, *7*, 1211.

(71) (a) Smith, M. B.; March, J. *March's Advanced Organic Chemistry Reactions, Mechanisms, and Structure*, 5th ed.; Wiley & Sons: New York, 2001; p 463. (b) Saloma, P. *The Chemistry of Carbonyl Group*; Wiley: New York, 1966; Vol. 1, p 177.

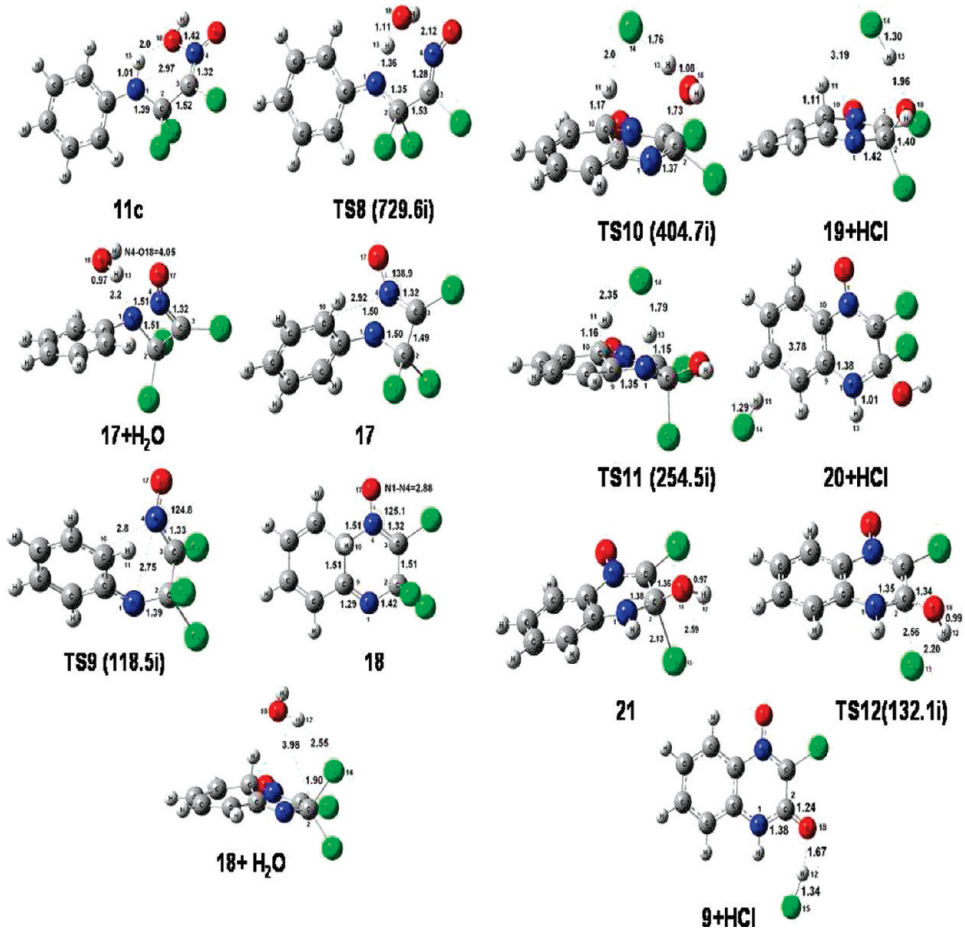

FIGURE 4. Optimized structures of transition states and intermediates for path 3. Imaginary frequencies are given in parentheses.

1.34, and 1.24 Å in structures **20**, **TS12**, and **9**, respectively. The activation barrier of the last step is very low, 0.5 kcal/mol, according to the Gibbs free energy values given in Figure 3.

For path 3, the WE step is the rate-determining step with a Gibbs activation energy of 31.9 kcal/mol. The overall reaction is extremely exothermic by about −80 kcal/mol. This path also supports experimental findings such as the exothermicity of the reaction and the fact that N-substituted anilines do not give the reaction since the second hydrogen atom of N1 is also abstracted in the rate-determining step.

3.5. Path 4. The initial stage of path 4 is HCl elimination followed by Michael addition. The elimination of HCl is exothermic with an early transition state (**TS13**), constituting strong intramolecular hydrogen bonds: N1···H12−O18 (1.56 Å) and N1−H13···Cl14 (2.03 Å). In this step, the C2−Cl14 bond length stretches from 1.87 Å in **11a** (Figure 1) to 2.77 Å in **TS13** (Figure 5), whereas the C2−N1 bond length shortens from 1.45 Å in **11a** (Figure 1) to 1.41 Å in **TS13** and 1.29 Å in **21** (Figure 5). The activation energy is about 13.8 kcal/mol, and the reaction energy is −17.2 kcal/mol according to the Gibbs free energy values in Figure 5. The second step is inversion of the N1 atom. The direction of the lone pair on the N1 atom changes, and this can be seen clearly in Figure 5. The C9−N1−C2−C3 dihedral angle changes from −177.2° in **21** to −91.3 and 5.8° in **TS14** and **22**, respectively. The Gibbs activation energy is predicted to be 20.2 kcal/mol, and the reaction energy is endothermic by 7.9 kcal/mol. The strong H-bonding interaction between N1 and H12 stabilizes **21** relative to **22**. The third step involves an electrocyclization reaction, which takes place through **TS15** to afford intermediate **23**, which is a very unstable structure. A potential energy surface scan for the electrocyclization step shows that the activation barrier is 45.4 kcal/mol, and the reaction is considerably endothermic by 35.7 kcal/mol. The reason is that the aromaticity of the benzene ring is destroyed because of the newly formed C10−N4 bond whose distance varies as 4.27, 2.13, and 1.54 Å in **22**, **TS15**, and **23**, respectively. Double bonds in **22**, C3−N4 (1.32 Å), N1−C2 (1.26 Å), and C9−C10 (1.41 Å), are converted to single bonds (1.51, 1.37, 1.51 Å, respectively), while the C3−C2 (1.48 Å) and C9−N1 (1.41 Å) single bonds turn into double bonds with bond lengths of 1.36 and 1.30 Å, respectively, as shown in Figure 5. After the electrocyclization step, the aromaticity of the benzene ring is gained back via elimination of a water molecule from **23** to produce quinoxaline-*N*-oxide (**24**). This step is highly exothermic with −91.9 kcal/mol and has a very low activation barrier, 7.3 kcal/mol, since the aromaticity is regenerated. In the transition state **TS16**, the hydroxy group attached to the N4 atom picks up proton H11 and leaves as water. The forward IRC calculation for **TS16** produces an intermediate complex between compound **24** and a water molecule, constituting a hydrogen bond. The H11−O18 bond distance shortens from 2.32 Å in **23** to 1.80 and 0.97 Å in **TS16** and the intermediate complex (**24**+$\mathbf{H_2O}$), respectively, while the N4−O18 bond (1.54 Å) in **23** stretches to 2.03 Å in **TS16**.

The rate-determining step of path 4 is electrocyclization with 45.4 kcal/mol (36.1 kcal/mol relative to **11a**) activation energy. The predicted barrier is too high for a reaction occurring at about room temperature. Besides, the hydrolysis of **24** to target product

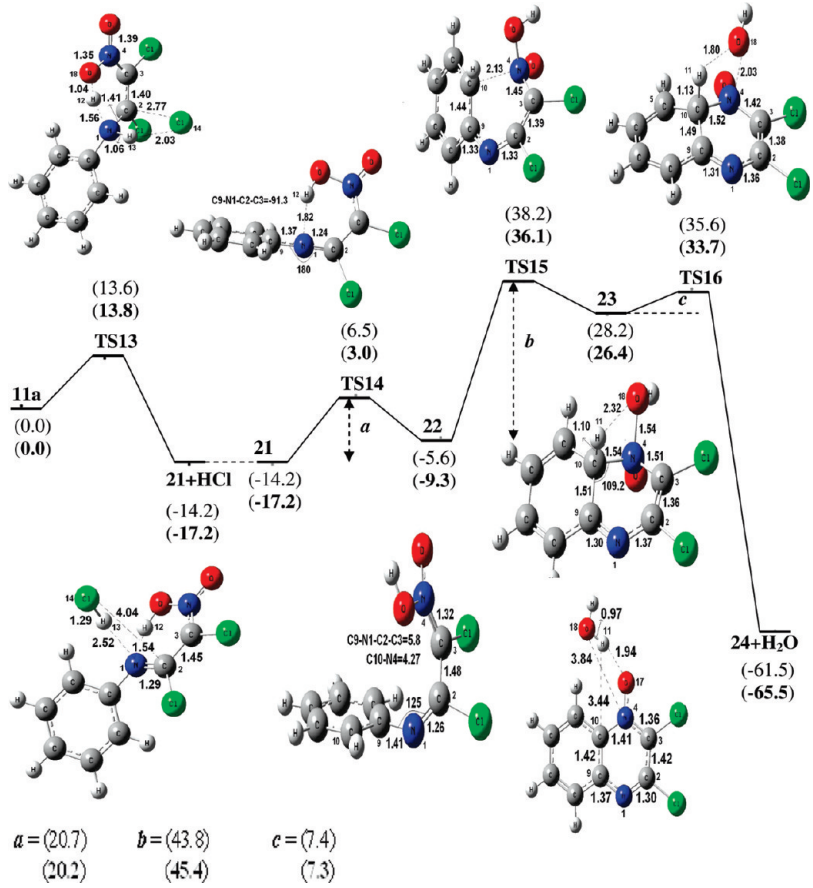

FIGURE 5. Energetics [ZPE corrected energy and Gibbs energy (bold), (kcal/mol)] and optimized structures in path 4.

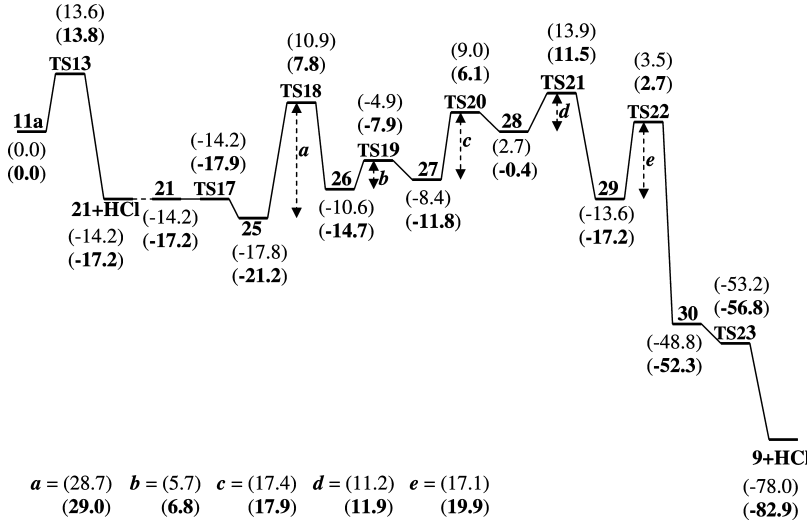

FIGURE 6. Energetics [ZPE corrected energy and Gibbs energy (bold), (kcal/mol)] and optimized structures in path 5.

9 was not modeled but was tested experimentally since 2,2-dichloro-(1*H*)-quinoxaline-*N*-oxide (**24**) is a very stable and commercially available compound. Since the actual synthesis of quinoxalinone-*N*-oxides is performed in methanol, this hydrolysis was also carried out in methanol. The reaction of **24** with water in methanol under basic conditions gave a 2-chloro-3-methoxyquinoxaline-4-oxide derivative (14% yield) instead of product **9**, suggesting that the reaction does not proceed via **24**. These experimental as well as computational findings provide negative evidence for path 4.

3.6. Path 5. Path 5 proceeds via a four-membered heterocyclic intermediate similarly to path 3 and involves eight steps after Michael addition of **1** to **8**. Energetics and optimized geometries are given in Figures 6 and 7, respectively. The first step is the same as the first step of path 4, in which the HCl elimination from **11a** takes place through **TS13**. The remaining steps are 1,5-H shift from O18 to N1 in **21**, *cis*−*trans* isomerization of **25**, conformational change from **26** to **27**, oxygen attack from N4 to C2 in order to produce four-membered ring intermediate **28**, rearrangement of **28**, cyclization and

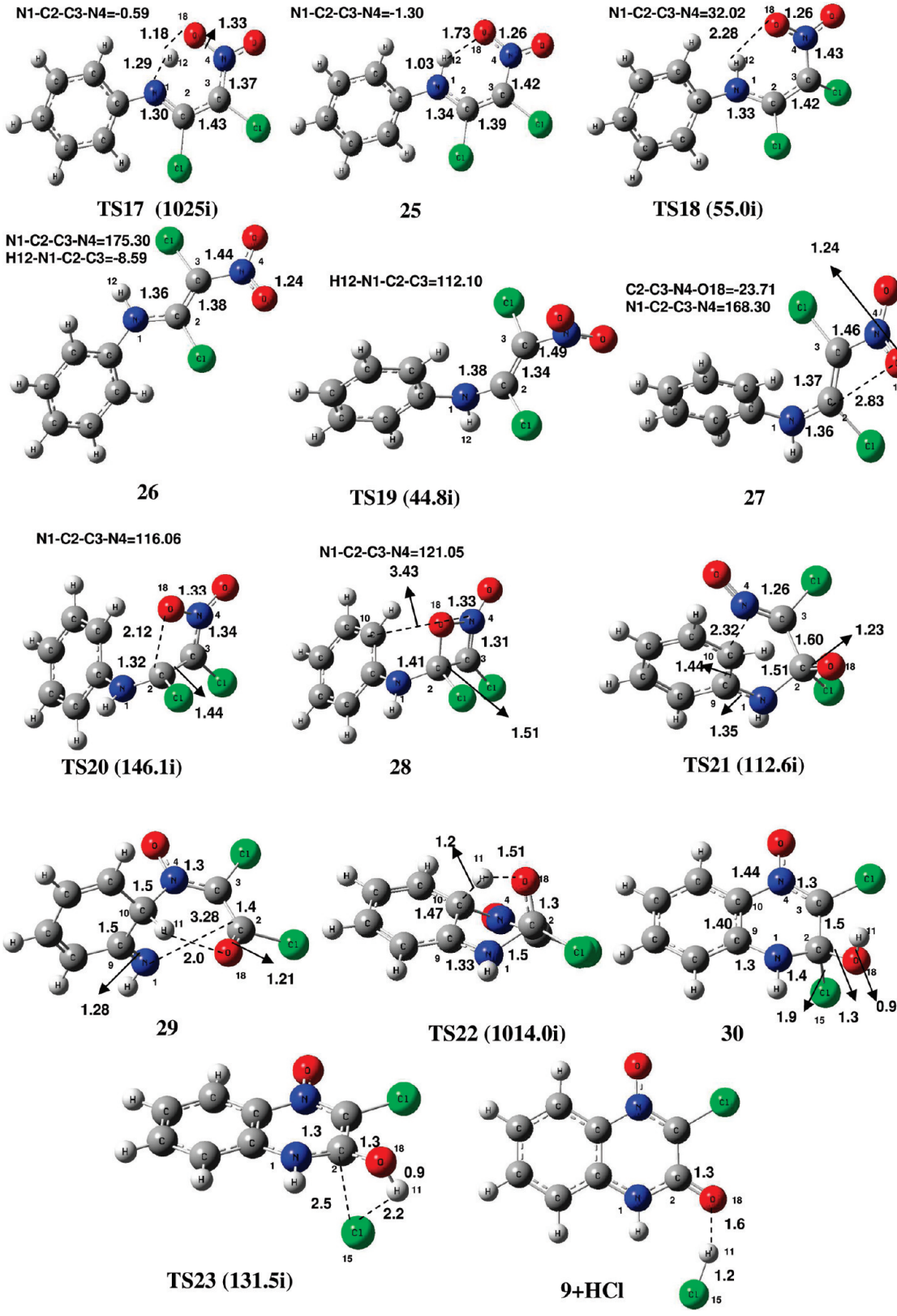

FIGURE 7. Optimized structures for path 5. Imaginary frequencies are given in parentheses.

hydrogen transfer from C10 to O18 in **29**, and finally elimination of HCl from **30** to produce product **9**. **TS17** is the transition state of the 1,5-H shift, in which the N1−H12 bond length shortens from 1.54 Å in **21** to 1.29 Å in **TS17** and 1.03 Å in **25** (Figure 7). Normal mode analysis of **TS17** shows that it has only one imaginary frequency of 1025.13*i* corresponding to the transfer of H12. Structure **25** shows N1−H12···O18 hydrogen bonding with 1.73 Å and is only 3.5 kcal/mol more stable than **21**. Interestingly, **TS17** is 0.9 kcal/mol more stable than intermediate **21**. One can expect that structures **21** and **25** can be interconverted in a dynamic equilibrium (Scheme 9) on the basis of the experimental observation of Rajappa et al.[72]

SCHEME 9

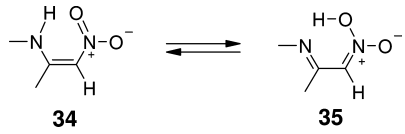

34 **35**

They observed a highly chelating OH and NH absorption in the IR spectra of nitroenamine derivatives, suggesting that both **34** and **35** would exist in the equilibrium. The barrierless reaction between **21** and **25**, predicted by B3LYP/6-31+G**, is in agreement with the above observation.

The transition state **TS18** of the *cis*−*trans* isomerization (CTI) step was generated with the coordinate-driving potential scan and optimized under the constraint of the N1−C2−C3−N4 dihedral angle. Normal mode analysis gave one imaginary frequency of 55.02*i* representing the rotation of C2−C3 bond. The peak height for the curve given in Figure 8 is 29.0 kcal/mol. This barrier is interestingly low compared to the known isomerization barrier of usual alkenes (∼62−65 kcal/mol).[73] This can be attributed to the push−pull effect of nitro and *N*-phenyl amino groups on the C2−C3 double bond in **25**, which leads to an increase in bond length and a decrease in isomerization barrier. As seen in Figure 7, the C2−C3 bond in **TS18** exhibits only partial double bond character with a bond length of 1.43 Å.

TS19 represents conformational change from **26** to **27**. Although the N1−C2 bond exhibits partial double bond character with a distance of 1.36 Å, rotation around the N1−C2 bond requires an activation barrier of only 6.8 kcal/mol. The H12−N1−C2−C3 dihedral angle is −8.59° in **26**, 112.10° in **TS19**, and 151.94° in **27**. In the next step, O18 attacks C2 to give four-membered heterocyclic intermediate **28**, a 1,4-dihydro-1,2-oxazete derivative, through transition state **TS20** with an activation energy of 17.9 kcal/mol. One can also think that the *cis* isomer of nitroenamine derivative **25** can turn into **TS20** directly to produce **28**. However, reverse IRC computation for **TS20** produces only the *trans* isomer, **27**, indicating that a *cis*−*trans* isomerization step is also required. In **TS20**, a new C2−O18 bond starts to form. While the C2−O18 distance is 2.83 Å in **27**, it shortens to 2.12 and 1.46 Å in **TS20** and **28**, respectively. The C2−C3 double bond (1.37 Å) and N4−O18 partial double bond (1.24 Å) in **27** are elongated to 1.44 and 1.33 Å in **TS20** and 1.51 and 1.53 Å in **28**, respectively.

Intermediates **25**, **26**, and **27** are nitroenamine structures that have been shown to be useful synthetic intermediates in organic synthesis.[74] Nitroenamine **27** is used in the formation of oxazete derivative **28** through oxygen transfer from the NO_2 group to the electrophilic carbon atom in this path. A similar intramolecular oxygen transfer was also reported in the rearrangements of 2-nitroenamines in acidic solutions (Scheme 10) by Krówczyński et al.[75]

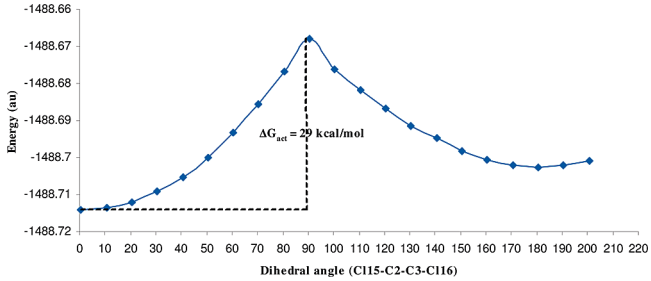

FIGURE 8. Potential energy scan for *cis*−*trans* isomerization step.

SCHEME 10

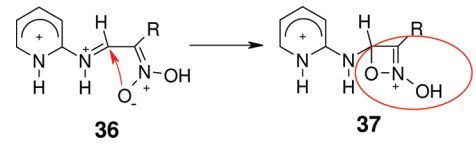

36 **37**

SCHEME 11

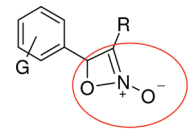

38

Additionally, Kassaee et al.[76] reported the formation of oxazete ring **38**. They investigated the effect of the substituent on the photochemistry of β-methyl-β-nitrostyrene and observed that the oxazete ring formed in the presence of an electron-withdrawing group on the benzene ring (Scheme 11).

The rearrangement of **28** produces **29**, an α,β-unsaturated acylchloride derivative, via **TS21**. In this step, the N1−C2 and O18−N4 single bonds break, while the C10−N4 single bond and the C2−O18 double bond form, and the aromaticity of the benzene ring disappears. It is seen from Figure 7 that the N1−C2 single bond (1.41 Å) in **28** stretches to 1.51 and 3.28 Å, while the C10−N4 distance in **28** shortens to 2.32 and 1.51 Å in **TS21** and **29**, respectively, suggesting that **TS21** is an early transition state. Therefore, the activation energy of this step is 11.9 kcal/mol, and the reaction is exothermic with −16.7 kcal/mol. The transformation of **28** to **29** involving **TS21** can be viewed as a Cope-like rearrangement in which, instead of the second allylic fragment, an oxazete residue is involved. **TS22** represents the nucleophilic attack of N1 on the C2 atom and abstraction of the H11 proton by O18. As a result, aromaticity is regenerated. An activation energy of 19.9 kcal/mol is needed to reach this transition state. Compound **29** is 35.1 kcal/mol less stable than **30**. The heterocyclic ring of structure **30** is not planar, but the necessary conditions for electron delocalization can be provided by HCl elimination from this structure. **TS23** is the transition state of this elimination, in which the Cl15−C2 (2.56 Å) and H11−O18 (0.99 Å) single bonds break, while the H11−Cl15 (2.20 Å) single bond and the C2−O18 (1.34 Å) double bond form. Surprisingly, the transition sate, **TS23**, is more stable (4.5 kcal/mol) than reactant **30** of this final step. This step is very exothermic by −30.6 kcal/mol.

Although the rearrangement step (**TS21**) seems to be the rate-determining step when the activation barrier is evaluated relative to **11a**, the rate-determining step of path 5 is considered to be the CTI step with an activation barrier of 29.0 kcal/mol since **TS18** requires a barrier that is only 3.5 kcal/mol lower than that of **TS21** but has the highest barrier relative to its reactant complex. Path 5 can also explain why N-substituted anilines do not give the annulation reaction since two hydrogen atoms at the nitrogen atom of aniline are required for this mechanism

(72) Rajappa, S.; Nagarajan, K.; Venkatesan, K.; Kamath, N.; Padmanabhan, V. M.; Philipsborn, W. V.; Chen, B. C.; Müller, R. *Helv. Chim. Acta* **1984**, *67*, 1669.
(73) Smith, M. B.; March, J. *March's Advanced Organic Chemistry Reactions, Mechanisms, and Structure*, 5th ed.; Wiley: New York, 2001; p 159.
(74) Rajappa, S. *Tetrahedron* **1981**, *37*, 1453.
(75) Krówczyński, A.; Kozerski, L. *Bull. Pol. Acad. Sci. Chem.* **1986**, *34*, 341.
(76) Kassaee, M. Z.; Nassari, M. A. *J. Photochem. Photobiol. A* **2000**, *136*, 41.

TABLE 2. Activation Energies (kcal/mol) and Relative Energies (in parentheses) for Rate-Determining Steps Calculated at 25 and 40 °C

WE step of path 3	$\Delta G^{\ddagger}$
298.15 K	31.928 (0.000)
313.15 K	31.927 (−0.001)
CTI step of path 5	$\Delta G^{\ddagger}$
298.15 K	28.977 (0.000)
313.15 K	29.008 (0.031)

TABLE 3. Activation Energies (kcal/mol) and Relative Energies (in parentheses) for Rate-Determining Steps Calculated in Methanol

WE step of path 3	$\Delta E^{\ddagger}$	$\Delta G^{\ddagger}$
gas phase	32.0 (0.0)	31.9 (0.0)
methanol	38.3 (6.3)	38.2 (6.3)
CTI Step of Path 5	$\Delta E^{\ddagger}$	$\Delta G^{\ddagger}$
gas phase	28.7 (0.0)	29.0 (0.0)
methanol	22.6 (−6.1)	22.9 (−6.1)

[in the HCl elimination step from **11a** and in the 1,5-H shift step (**TS17**)]. The overall reaction is highly exothermic by −82.9 kcal/mol. These results indicate that path 5 is a plausible mechanism of the annulation reaction given in Scheme 2.

Among the modeled mechanisms, path 3 and path 5 were found to be the most plausible ones since the difference between the activation energies in their rate-determining steps was only 2.9 kcal/mol. As it was reported that the B3LYP/6-31+G** method overestimates the activation enthalpies by about 3 kcal/mol in the methylene nitrone reactions,[57] the actual barriers in paths 3 and 5 are expected to be a few kcal/mol less than the predicted values. In addition, experimental evidence suggests that several parameters, such as substituent, temperature, and solvent, also affect the reaction yield,[21,22] so the activation barriers of these paths might also be influenced by these parameters. Therefore, the effects of these parameters on the rate-determining steps of paths 3 and 5 were also investigated.

3.7. Temperature Effects. Frequency computations were carried out to calculate thermodynamic properties at 25 °C. However, experimentally, the optimum reaction temperature was determined to be 40 °C. Therefore, the temperature effect was included in computing the activation energies of the rate-determining steps of paths 3 and 5. Nevertheless, as seen in Table 2, no substantial difference between the activation barriers was observed at 25 and 40 °C.

3.8. Solvent Effects. The proposed mechanisms were modeled in the gas phase, whereas the reaction was carried out mainly in methanol. It is expected that the solvation effect can stabilize the transition states and assist the reaction. Therefore, the effect of the solvent was taken into consideration by calculating the activation barriers of the WE and CTI steps of path 3 and path 5, respectively, by using the self-consistent reaction field theory in methanol. These values are listed in Table 3.

For the WE step of path 3, an increase (6.3 kcal/mol) in the activation energy was observed, whereas a decrease by 6.1 kcal/mol was observed for the CTI step of path 5. The increase in the barrier of the WE arises from the fact that **11c** has a higher dipole moment than **TS8** (Table 4). However, the barrier lowering by methanol for path 5 makes it a more likely candidate.

3.9. Effects of Computational Methods and Basis Sets. Activation barriers of the rate-determining steps (WE and CTI) of chosen paths (3 and 5) were predicted to be 31.9 and 29.0 kcal/mol, respectively, by B3LYP/6-31+G**. In order to see how other computational methods would affect these barriers, B3LYP/6-31+G** was compared to the PBE1PBE,[70] BLYP,[71] B3PW91,[72] MPW1PW91,[73] MPW1K,[62] and MP2(SP) methods by using 6-31+G** and different basis sets (6-31G*, 6-31G**, and 6-31++G**) with B3LYP.

TABLE 4. Dipole Moments of the Reactants and Transition States in the Rate-Determining Steps of Path 3 and Path 5

WE Step of Path 3	μ
11c	3.23
TS8	2.16
CTI step of path 5	
25	6.34
TS18	8.25

TABLE 5. Activation Energies of the WE and CTI Steps and Relative Energies (in parentheses) with respect to B3LYP/6-31+G Level**

computational methods	WE step of path 3		CTI step of path 5	
	$\Delta E^{\ddagger}$	$\Delta G^{\ddagger}$	$\Delta E^{\ddagger}$	$\Delta G^{\ddagger}$
B3LYP/6-31G*	34.4 (2.4)	34.1 (2.2)	34.5 (5.8)	34.7 (5.7)
B3LYP/6-31G**	32.8 (0.8)	32.6 (0.7)	34.9 (6.2)	35.0 (6.0)
B3LYP/6-31+G**	32.0 (0.0)	31.9 (0.0)	28.7 (0.0)	29.0 (0.0)
B3LYP/6-31++G**	32.1 (0.1)	32.0 (0.1)	28.7 (0.0)	29.0 (0.0)
BLYP/6-31+G**	32.0 (0.0)	31.9 (0.0)	26.6 (−2.1)	27.7 (−1.3)
B3PW91/6-31+G**	34.5 (2.5)	34.6 (2.7)	29.5 (0.8)	29.8 (0.8)
MP2(SP)/6-31+G**// B3LYP/6-31+G**	41.3 (9.3)	41.2 (9.3)	29.5 (0.8)	29.8 (0.8)
PBE1PBE/6-31+G**	39.1 (7.1)	39.2 (7.3)	30.0 (1.3)	30.3 (1.3)
MPW1PW91/6-31+G**	35.8 (3.7)	35.8 (3.9)	29.9 (1.2)	30.2 (1.2)
MPW1K/6-31+G**	52.1 (20.1)	51.9 (20.0)	26.5 (−2.2)	26.3 (−1.7)

We observed different trends in path 3 and path 5, as shown in Table 5. For path 3, increasing or decreasing the size of basis set did not considerably influence the barriers. Only 6-31G* estimated a higher barrier (by 2.4 kcal/mol) than 6-31+G**. Activation energies calculated with the BLYP method were very closer to those calculated by B3LYP, whereas the PBE1PBE, MPW1PW91, and MP2(SP) methods produced higher activation energies than the chosen level by 7.0, 3.7, and 9.2 kcal/mol, respectively. Interestingly, the MPW1K method overestimated the barrier by 20.0 kcal/mol. For the CTI step of path 5, addition of a second set of diffusion functions to B3LYP/6-31+G** did not change the energies. Decreasing the size of the basis set for B3LYP increased the activation barriers by about 6 kcal/mol. Single point MP2 computations and the B3PW91 method estimated activation energies that were 0.8 kcal/mol higher than those estimated by B3LYP. The PBE1PBE and MPW1PW91 methods overestimated the barrier by 1.2 kcal/mol, whereas the BLYP and MPW1K methods underestimated the activation energies by 2.1 and 2.2 kcal/mol, respectively.

It is interesting that the MPW1K method gave very different predictions in our calculations. Truhlar et al.[59] stated that MPW1K predicted the best barrier heights for a set of 22 reactions whose experimental kinetic data are known and recommended the 6-31+G** basis set. Houk et al.[57] reported that the MPW1K method performed better than B3LYP in estimating the activation barriers of a set of 1,3-dipolar cycloaddition reactions, but the 6-31G* basis set showed better performance than 6-31+G*. In our case, the MPW1K method predicted a higher activation barrier for the WE step in path 3 but lower for the CTI step in path 5 relative to B3LYP, and the 6-31+G** basis set predicted better barriers than 6-31G*. However, many articles in the literature support that MPW1K

TABLE 6. Product Yields under Identical Conditions

substituent of the introduced aniline	yields (%)
H	63
m-OMe	65
p-OMe	51
p-F	16
p-Cl	42
m-Cl	9

TABLE 7. Substituent Effects on the Activation Energies (kcal/mol) and Relative Energies with Respect to Hydrogen (in parentheses)

	WE step of path 3		CTI step of path 5	
substituent	$\Delta E^{\ddagger}$	$\Delta G^{\ddagger}$	$\Delta E^{\ddagger}$	$\Delta G^{\ddagger}$
p-NH_2	27.3 (−4.7)	27.1 (−4.8)	31.8 (3.1)	32.2 (3.2)
p-OH	29.5 (−2.5)	29.5 (−2.4)	28.2 (−0.5)	28.5 (−0.5)
p-OMe	29.1 (−2.9)	29.0 (−2.9)	32.3 (3.6)	32.1 (3.1)
p-CH_3	31.0 (−1.1)	31.0 (−0.9)	28.4 (−0.3)	29.2 (0.2)
p-F	31.3 (−0.7)	31.2 (−0.7)	32.7 (4.0)	33.1 (4.1)
p-Cl	31.3 (−0.7)	31.3 (−0.6)	29.0 (0.3)	29.1 (0.1)
p-Br	31.2 (−0.8)	31.1 (−0.8)	29.1 (0.4)	29.2 (0.2)
H	32.0 (0.0)	31.9 (0.0)	28.7 (0.0)	29.0 (0.0)
p-COOH	32.9 (0.9)	33.0 (1.1)	29.6 (0.9)	29.7 (0.7)
p-CN	32.5 (0.5)	32.6 (0.7)	34.0 (5.3)	34.1 (5.1)
p-NO_2	33.3 (1.3)	33.3 (1.4)	34.5 (5.8)	34.7 (5.7)
m-OMe	32.1 (0.1)	32.0 (0.1)	28.7 (0.0)	28.6 (−0.4)
m-Cl	32.3 (0.3)	32.3 (0.4)	33.3 (4.6)	33.6 (4.6)

produces the most accurate saddle point geometries, estimates very close energies to experimental values, and is a more reliable method than B3LYP.[77]

To sum up, the estimated activation energy for the CTI step of path 5 varies between 26.2 and 34.6 kcal/mol, while that for the WE step of path 3 is between 31.9 and 51.9 kcal/mol. When the prediction of a more reliable method (MPW1K) and the solvation effect are considered collectively, a lowering of at least 8 kcal/mol in the barrier of the CTI step will result in an activation barrier of about 20 kcal/mol. In addition, the energy evolved in previous exothermic steps (totally about −19 kcal/mol) can also be used to overcome this barrier. Overall, these data provide strong evidence that path 5 is a plausible mechanism for the annulation reaction.

3.10. Substituent Effects. Kaufmann et al.[22] investigated the substituent effect by using six aniline derivatives under identical reaction conditions and reported that the yields of **9** depended strongly on the substituent of the introduced anilines, ranging from 9 to 65% (Table 6).

It was also stated that both electron-withdrawing groups, such as F and Cl, at C6 and electron-donating groups, such as methoxy, at C6 or C7 had a negative effect on the reaction yield. This finding suggests that a relationship does not exist between the electronic nature of the substituent and the outcome of the reaction. In order to see which path is consistent with this experimental observation, substituent effects on the rate-determining steps (WE and CTI) of both path 3 and path 5 were studied; the results are listed in Table 7. The relationships of the activation energies with the Hammett constants[78] (σ) of

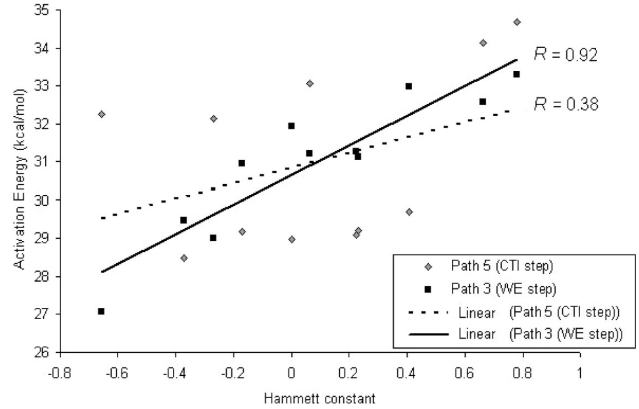

FIGURE 9. Correlation plot of computed activation energies vs Hammett constants.

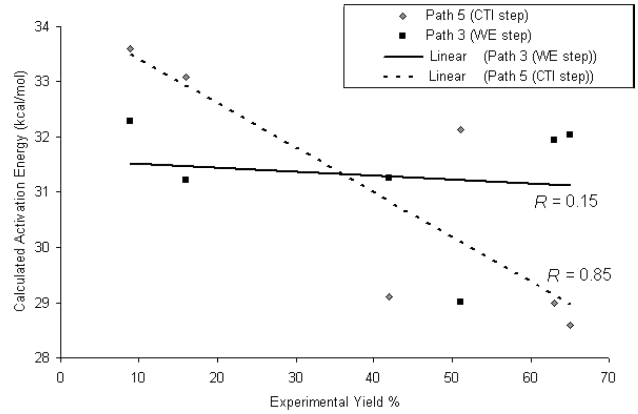

FIGURE 10. Correlation plot of computed activation energies vs reaction yields.

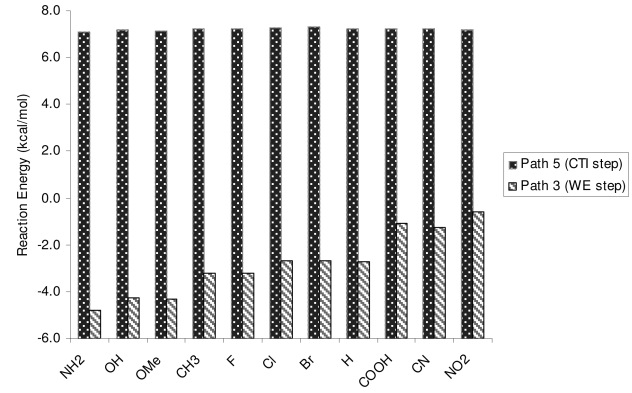

FIGURE 11. Comparison of reaction energies of the WE and CTI steps for various substituents.

substituents and the experimental reaction yields were also investigated.

For the WE step of path 3, electron-donating groups were found to reduce the activation energy (Table 7). The largest decrease in the activation energy amounts to 4.8 kcal/mol for the substituent group NH_2. On the other hand, electron-withdrawing groups increase the activation energy. The NO_2 group causes a deactivation by 1.4 kcal/mol. Computed Gibbs activation energies had a good correlation ($R = 0.92$) with the Hammett constant of the substituent (σ) (Figure 9) but did not have any correlation with the experimental reaction yields (Figure 10). The reaction energy (Figure 11) showed similar trends as the activation energy for the WE step.

(77) (a) Rybtchinski, B.; Oevers, S.; Montag, M.; Vigalok, A.; Rozenberg, H.; Martin, J. M. L.; Milstein, D. *J. Am. Chem. Soc.* **2001**, *123*, 9064. (b) Dibble, T. S. *J. Phys. Chem. A* **2002**, *106*, 6643. (c) Voegele, A. F.; Tautermann, C. S.; Loerting, T.; Liedl, K. R. *J. Phys. Chem. A* **2002**, *106*, 7850. (d) Ren, Y.; Wolk, J. L.; Hoz, S. *Int. J. Mass Spectrom.* **2002**, *221*, 59. (e) Claes, L.; Francois, J. P.; Deleuze, M. S. *J. Comput. Chem.* **2003**, *24*, 2023.

(78) Hammett, P. L. *Physical Organic Chemistry: Reaction Rates, Equilibria, and Mechanisms*, 2nd ed.; McGraw-Hill: New York, 1970; Chapter 11, pp 347−390.

In path 5, *p*-OH and *m*-OMe groups decrease the barrier of the CTI step; however, NH_2, OMe, F, CN, and NO_2 groups at the *para* position and a Cl atom at the *meta* position cause an increase in this barrier. As shown in Figure 9, there is no correlation between the activation energies and the Hammett constants. This is consistent with experimental observation. On the other hand, Figure 10 shows a correlation (with a negative slope) between the activation energy and the reaction yields ($R = 0.85$). The agreement between the available experimental data and the computations provides significant support for path 5. This correlation suggests that the reaction yield depends on the activation barrier in such a way that the barrier increases as the yield decreases. As shown in Figure 11, no significant change in reaction energies with respect to the type of substituent was observed. The existence of a correlation with the activation barriers but not with the reaction energies indicates that the annulation reaction is kinetically controlled. The substituent effects as well as other parameters investigated also indicate that path 5 is the most plausible mechanism for the annulation reaction of TCNiE with aniline among the mechanisms proposed.

4. Conclusion

The above results are obtained by the first computational study of the potential energy surface of the annulation mechanism of trichloronitroethylene and aniline, resulting in the synthesis of a new quinoxalinone-*N*-oxide derivative. After Michael addition, five different paths (1−5) have been proposed here and modeled by using density functional theory. The potential energy surfaces give rise to very interesting intermediate species **17** and **28**, which have also been proposed for several other reactions.[32,68,69] The following conclusions can be drawn from this study:

1. According to the model study (Scheme 6), MP2 and DFT(B3LYP) show a similar trend in the estimation of the reaction energy.

2. For paths 1 and 2, proposed by Kaufmann et al.,[21] the transition state and intermediate of electrophilic aromatic substitution step in path 1 could not be optimized, and path 2, based on the aza-Cope rearrangement, generated a very high activation energy in the rate-determining step. In addition, path 2 cannot explain why N-substituted aniline does not give the reaction.

3. Although path 3 occurring at 40 °C and verifies the fact that the reaction is exothermic, the effects of the solvent, computational methods, and substituents do not agree with the experimental observations.

4. Path 4 is not a plausible mechanism, as path 2, since it requires a higher activation barrier compared to paths 3 and 5. The experimental support for this result is that the hydrolysis of intermediate **24** does not give target product **9**.

5. Path 5 is the most plausible mechanism since it has reasonable activation barriers and supports all experimental observations.

As one reviewer suggested, an alternative to the path from **11a** to **26** through **TS13**, **TS17**, and **TS18** would involve the transformation of **11a** to its nitro form (a prototropic tautomer) that undergoes the elimination of HCl to produce **26** directly, thus avoiding an unlikely *cis*−*trans* isomerization of **25** to **26**. This path, shown in Scheme S1 in the Supporting Information, was modeled using B3LYP/6-31+G** level. The results and the potential energy surface are given in Supporting Information. The first step involving tautomerization from **11a** to **31** was found to have an activation barrier of 42.4 kcal/mol (Figure S9 and Table S6 in Supporting Information). Although the HCl elimination step proceeds readily, the energy barrier of the tautomerization step (rate determining) is very high. Thus, this proposed path does not appear to be plausible.

Acknowledgment. We would like to acknowledge the Marmara University Scientific Research Commission, Project No. FEN-DKR-041200258, and the Turkpetrol Foundation for financial support. We also thank Prof. Dr. Viktoria Aviyente and Prof. Dr. Carl Trindle for their valuable suggestions.

Supporting Information Available: Optimized Cartesian coordinates, energies of all stationary points, information on additional path, and complete citation for refs 60 and 61. This material is available free of charge via the Internet at http://pubs.acs.org.

JO9003629